Towards an Integrated QR Code Biosensor: Light-Driven Sample Acquisition and Bacterial Cellulose Paper Substrate

Mingquan Yuan, *Student Member, IEEE*, Qisheng Jiang, Keng-Ku Liu, Srikanth Singamaneni, and Shantanu Chakrabartty, *Senior Member, IEEE*

***Abstract*—This paper addresses two key challenges toward an integrated forward error-correcting biosensor based on our previously reported self-assembled quick-response (QR) code. The first challenge involves the choice of the paper substrate for printing and self-assembling the QR code. We have compared four different substrates that includes regular printing paper, Whatman filter paper, nitrocellulose membrane and lab synthesized bacterial cellulose. We report that out of the four substrates bacterial cellulose outperforms the others in terms of probe (gold nanorods) and ink retention capability. The second challenge involves remote activation of the analyte sampling and the QR code self-assembly process. In this paper, we use light as a trigger signal and a graphite layer as a light-absorbing material. The resulting change in temperature due to infrared absorption leads to a temperature gradient that then exerts a diffusive force driving the analyte toward the regions of self-assembly. The working principle has been verified in this paper using assembled biosensor prototypes where we demonstrate higher sample flow rate due to light induced thermal gradients.**

***Index Terms*—Automatic reagent sampling, bacterial cellulose, flexible electronics, forward error-correcting biosensor, lab-on-chip, mobile health, QR code, self-assembly, silver enhancement, self-powered sensing.**

I. Introduction

PAPER-BASED microfluidics provide an ultra-low cost platform to implement biosensors for portable point-of-care (POC) diagnostics and for on-site detection [1], [2], with applications ranging from immunoassays [3], urinalysis [4], environmental monitoring [5] to food safety [6]. When integrated with low-cost tagging technologies like radio-frequency identification (RFID) [7]–[9] or quick response (QR) codes [10], paper-based microfluidics platform could facilitate end-to-end food supply chain monitoring where food-packages can be endowed with biosensing capabilities. In our previous work we had demonstrated that both RFID tags [11], [12] and QR codes [10] can not only be used for encoding the static product information, but also can be used for monitoring target analytes. The decoding of both RFID biosensor and QR code biosensors can be performed using a smart-phone, either by using an integrated RFID or QR code scan capability. In this paper we address two specific challenges in integrating a paper-based QR code biosensor for food-supply chain monitoring.

The first challenge lies in the choice of the paper substrate on which the biosensor could be printed and assembled. In literature, Whitman filter-paper [4], [13] or nitrocellulose [14], [15] have been extensively used as paper substrates for biosensors. In this study, we have explored the use of bacterial cellulose as the substrate to fabricate the QR code biosensor. Bacterial cellulose is a biocompatible and bioactive material that has been approved by the US Food and Drug Administration (FDA) for the usage in clinical indications [16]. As a substrate it is attractive due to its open nanoporous structure, simple surface chemistry, excellent mechanical properties, low cost and scalable synthesis [17], [18]. Even under vigorous mechanical agitation and harsh chemical conditions, bacterial cellulose still exhibits excellent stability. These features of bacterial cellulose have been previously used for designing flexible Surface Enhanced Raman Scattering (SERS) substrate which shows ideal capabilities for bacteria collection [19]. In this paper, we show that bacterial cellulose also demonstrate excellent ink retention capability that ensures the printed QR code is stable when subjected to liquid analytes.

Another feature of bacterial cellulose substrate is that when the substrate is combined with an integrated absorbing graphene-oxide layer, a bacterial cellulose based bio-foam can also demonstrate excellent heat retention property [20]. We have used this property to address the second challenge related to the assembly of the QR code biosensor. Like any other paper-based biosensor, the QR code biosensor needs to acquire the target sample and direct the analyte into sensing region where the reagents are present. In a conventional sampling process, the reagent is physically applied (using a pipette or a dipstick [21]) to the paper substrate. While this sampling approach is convenient for cases when the analyte can be directly accessed, it is

Manuscript received September 25, 2017; revised December 16, 2017; accepted January 29, 2018. This work was supported by the National Science Foundation under Research Grant CCF: 1533905. This paper was recommended by Associate Editor D. Hall. *(Corresponding author: Shantanu Chakrabartty.)*

M. Yuan is with the Department of Computer Science and Engineering, Washington University in St. Louis, St. Louis, MO 63130 USA (e-mail: mingquan@email.wustl.edu).

Q. Jiang, K.-K. Liu, and S. Singamaneni are with the Department of Mechanical Engineering and Materials Science, Washington University in St. Louis, St. Louis, MO 63130 USA (e-mail: qjiang@wustl.edu; keng-ku.liu@wustl.edu; singamaneni@wustl.edu).

S. Chakrabartty is with the Department of Electrical and Systems Engineering, Washington University in St. Louis, St. Louis, MO 63130 USA (e-mail: shantanu@wustl.edu).

Color versions of one or more of the figures in this paper are available online at http://ieeexplore.ieee.org.

Digital Object Identifier 10.1109/TBCAS.2018.2801566

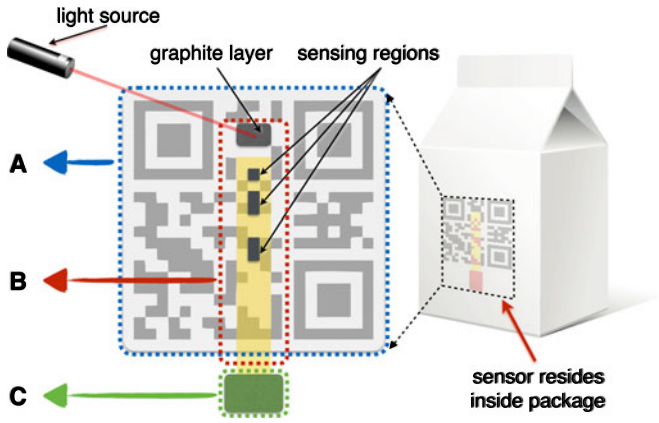

Fig. 1. Different components of a QR code biosensor that can be integrated on a liquid package and the sample acquisition could be triggered using a laser light source: component **A** shows a QR code which will be assembled based on detection; component **B** highlights the paper-based microfluidics channel part that could be integrated on **A** to remotely acquire liquid sample or reagent from a sample container **C** with a light source.

impractical for cases where the analyte is packaged or sealed, as shown in Fig. 1. In this paper we use a graphite-layer integrated with the Whatman filter paper substrate as a light-absorbing material for generating thermal gradients across a microfluidic channel, as shown in Fig. 1 and reported in [22]. The thermal gradient results in an increase in the diffusion rate that pushes the analyte into the region of interest.

The paper is organized as follows: Section II introduces QR code biosensor operating principle which is followed with materials and methods used to prepare the biosensor and the experimental setup. Four different substrates, including regular printing paper, Whatman filter paper, nitrocellulose membrane and lab synthesized bacterial cellulose, are used for the QR code biosensor prototype fabrication. This section also presents measurements obtained using the fabricated biosensor prototypes. In Section III a light absorption based analyte sampling approach has been proposed and verified on the Whatman filter paper substrate, and Section IV concludes the paper with discussions of future work.

II. QR Code Biosensor Substrates

A. Operating Principle of QR Code Biosensor

The principle of QR-code biosensor based on silver-enhancement self-assembly has been described in [10] and is summarized here and in Fig. 2 for the sake of completeness. A QR code is a two dimensional bar-code that encodes the product information along with an in-built error-correcting and alignment capability. When some of the QR code components (highlighted by black modules in Fig. 2(a)) are missing, the product information cannot be successfully retrieved. In [10] we self-assemble the modules using a process of silver-enhancement in the sensing regions as shown in Fig. 2. Silver enhancement based analyte detection relies on the formation of a sandwich structure comprising of primary probe (e.g., antibodies), target analyte and gold nanorod (AuNR) conjugated secondary probe. The AuNR conjugated secondary probes first hybridize with their target analytes which then bind with the primary probes that are immobilized in the sensing regions, as shown in Fig. 2(c). Any unbounded secondary probes are washed away leaving the sandwich structure (with AuNR label) intact. Because the dimensions of AuNRs are in a scale of nanometers, they are not large enough to be optically visible. When the silver enhancement solution is applied, silver ions start reducing into metallic silver on the surface of AuNRs, as shown in Fig. 2(d). As time progresses, more silver ions are reduced and deposited, and a chain of AuNRs cored silver micro-structures assemble. Thus, the regions where the silver-enhancement occurs become darker, illustrated in Fig. 2(e). In this way, an invalid QR codeword (Fig. 2(a)) transits into a valid codeword (Fig. 2(e)) which can be successfully decoded using a standard smartphone. We have previously verified that longer time is needed to assemble a valid QR code to detect target analyte with low concentration levels (shown in Fig. 2(f)). In the next section we investigate the use of bacterial cellulose susbtrate for integrating the QR code biosensor. Note that in [12], we have already described different techniques to construct and optimize the microfluidic channels using nitrocellulose membrane, and is omitted in this paper.

B. Materials and Methods

1) Materials and Apparatus: Gold chloride ($HAuCl_4$), Hexadecyltrimethylammonium bromide (CTAB), sodium borohydride ($NaBH_4$), silver nitrate ($AgNO_3$), ascorbic acid and silver enhancement kit were purchased from Sigma-Aldrich (St. Louis, MO, USA). *Gluconacetobacter hansenii* (ATCC 53582) and *Acetobacter xylinum* medium (ATCC 1765) were obtained from American Type Culture Collection (Manassas, Virginia, USA). Deionized water used in the experiment was obtained through Millipore water purification systems (Billerica, MA, USA). An EPSON stylus C88+ ink-jet printer was used to print the QR code. The printing substrates include multi-use printing paper from Boise Paper, grade 40 ashless Whatman filter paper from GE Healthcare (Little Chalfont, Buckinghamshire, UK), HF13504XSS nitrocellulose membrane from Millipore (Billerica, MA, USA) and lab synthesized bacterial cellulose. Truecolor 009 Gel pen were bought from eBay Inc to dispense the AuNR ink. 808 nm Laser Diode Control Units (LDCU 12) from Power Technology was used as light source to trigger the reagent flow. All the chemicals were used as received without further purification. The experiments were carried out in a certified Biological Safety Level II laboratory.

2) Synthesis of Bacterial Cellulose: Fig. 3 shows the schematic illustration of bacterial cellulose fabrication process. *Gluconacetobacter hansenii* (ATCC 53582) was cultured in test tubes containing 16 ml of #1765 medium at 30 °C under shaking at 250 rpm. The #1765 medium is composed of 2 % (w/v) glucose, 0.5 % (w/v) yeast extract, 0.5 % (w/v) peptone, 0.27% (w/v) disodium phosphate, and 0.5 % (w/v) citric acid. Bacterial culture solution (incubated 3 days) was added to the medium to make a total 7 ml solution. The solution was subsequently transferred to petri dish and incubated at room temperature without disturbance as shown in Fig. 3(a). After 5 days, a thin film of bacterial cellulose was formed. For purification,

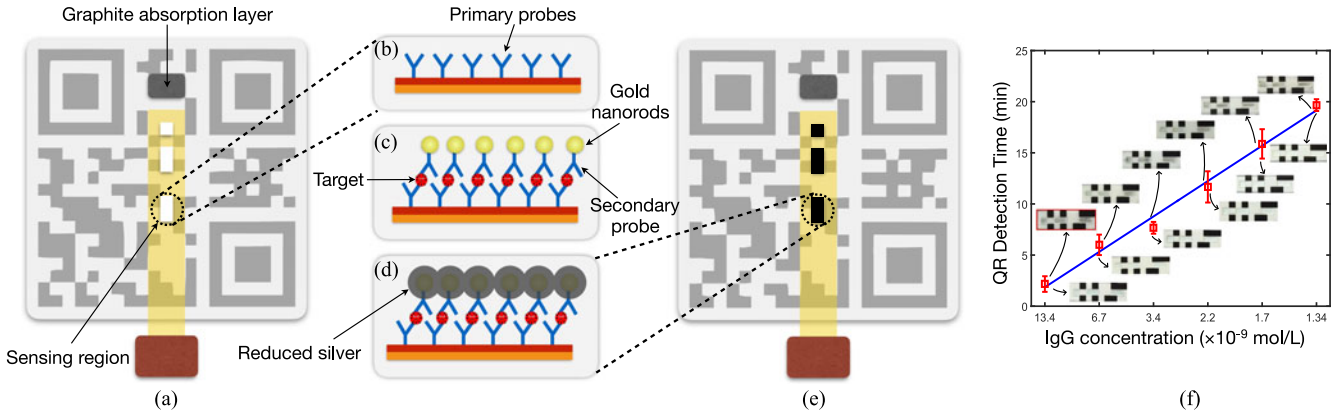

Fig. 2. Principle of QR code self-assembly and biosensing using silver enhancement. (a) QR code sensor before target detection; (b) primary probes specific to the target analytes immobilized in the sensing regions; (c) target analytes captured on primary probes; (d) silver enhancement technique used to assemble the parts of the QR code as shown in (e); (f) summarize previous experimental results showing that longer time is needed to assemble the QR code for the target with low concentration levels [10].

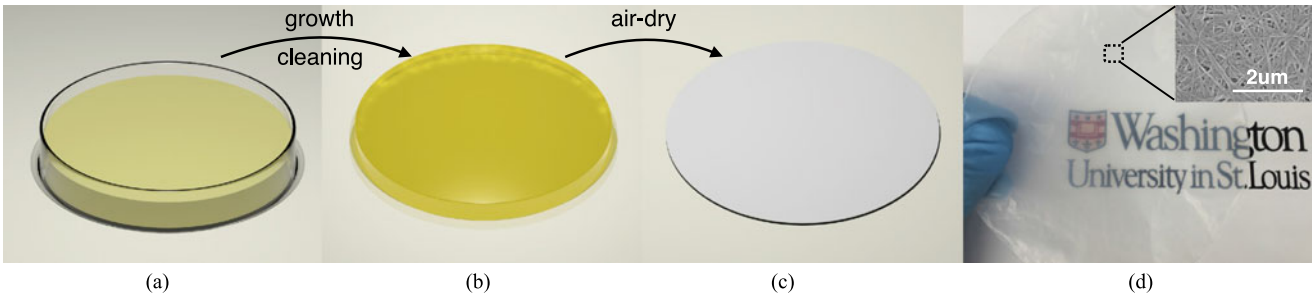

Fig. 3. Schematic illustration bacterial cellulose growth process: (a)–(c) schematic illustration showing bacterial paper synthesis process; (d) photo of synthesized bacterial cellulose (inset: SEM image showing surface morphology of bacterial cellulose).

the film was harvested from the petri dish and washed in a 500 ml of 0.1 M NaOH aqueous solution under boiling condition for 2 h. The obtained bacterial cellulose hydrogel (schematic illustrated in Fig. 3(b)) was then dialyzed in DI water for 2 days. The purified bacterial cellulose hydrogel was then air dried. Photo of the as synthesized bacterial cellulose is shown in Fig. 3(d).

3) Synthesis of AuNRs: AuNRs were synthesized by using seed-mediated method [23], [24]. Seed solution was synthesized by adding 0.6 ml of an ice-cold $NaBH_4$ (10 mM) solution into 10 ml of $HAuCl_4$ (0.25 mM) and CTAB (0.1 M) solution under vigorous stirring at room temperature. The color of the seed solution changed from yellow to brown. Growth solution was prepared by mixing 5 ml $HAuCl_4$ (10 mM), 95 ml CTAB (0.1 M), 1 ml $AgNO_3$ (10 mM) and 0.55 ml ascorbic acid (0.1 M), consecutively. The solution was homogenized by gentle shaking. To the resulting colorless solution, 0.12 ml of freshly prepared seed solution was added and kept undisturbed in the dark for 14h. Prior to use, the AuNR solution was centrifuged twice at 8000 rpm for 10 min to remove excess CTAB and re-dispersed in DI water. UV-Vis extinction spectrum was measured using Shimadzu UV-1800 UV-Vis spectrophotometer and shown in Fig. 4. The extinction spectrum of AuNR exhibits two characteristic bands at 510 nm and 794 nm, which corresponding to the transverse and longitudinal plasmon resonances, respectively. The length and diameter of AuNR were respectively measured to be 58.7 $\pm$ 4.5 nm and 14.5 $\pm$ 1.0 nm using Transmission electron

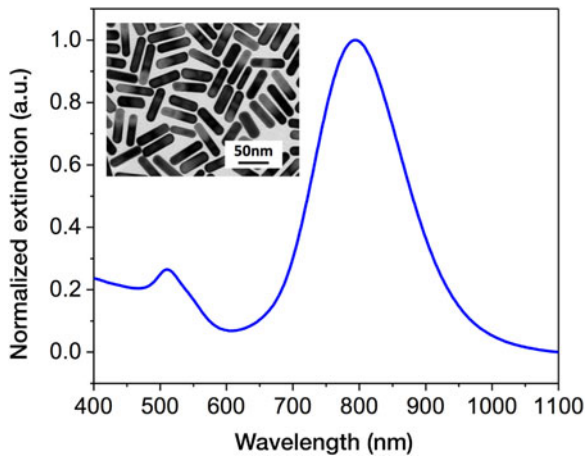

Fig. 4. Vis-NIR extinction spectrum of AuNR (inset: TEM image of AuNR).

microscopy (TEM) (inset in Fig. 4). TEM image was collected using a JEOL JEM-2100F field emission microscopy.

C. QR Biosensor Prototype Fabrication

The invalid or unassembled QR code is firstly printed on the substrate using EPSON C88+ printer with normal black ink, as shown in Fig. 5(a). We have used four different substrates in this paper, including regular printing paper, Whatman filter

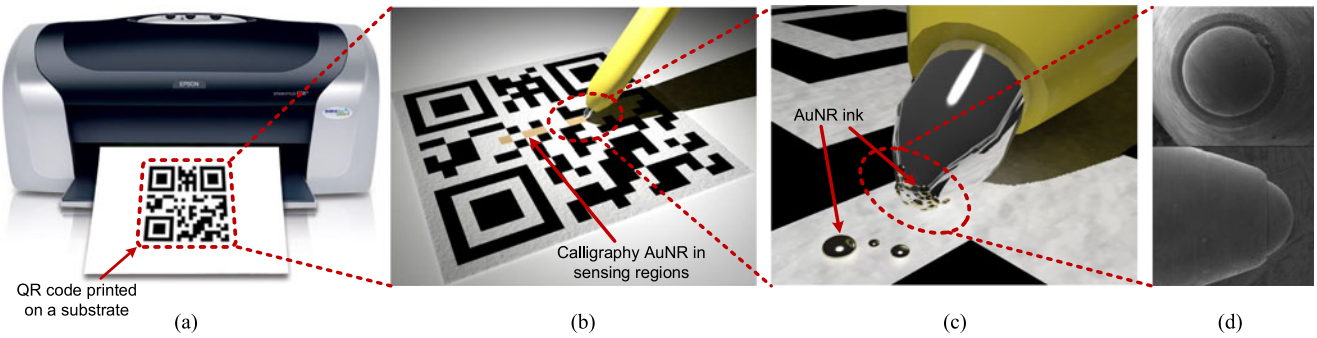

Fig. 5. Schematic illustration showing QR code biosensor fabrication procedure: (a) print the predefined QR code (invalid) on the substrate with normal black ink; (b) AuNR ink filled in the gel pen and dispensed on the self-assembling region; (c) schematic diagram showing AuNR ink drops on the pen tip surface; (d) SEM images of top view and side view of the pen tip.

paper, nitrocellulose membrane and lab synthesized bacterial cellulose. Once the printed QR code patterns are dried, AuNR ink is dispensed in the self-assembling regions where the five black modules have been intentionally removed (Figs. 2(a) and 5(b)). Although AuNRs have advantages over gold nanospheres (AuNPs) in some specific applications [25], [26], in this specific application it serves as a catalyst and facilitates the silver ion reduction process in silver enhancement to assemble the corrupted code-words. AuNPs can work in a similar manner to facilitate this process, which has been used to assemble RF antennas as reported in our previous work [7], [11], [12]. To dispense the AuNR ink in the self-assembling region more efficiently, ink-jet printing technique has been tried and reported in our previous work [10]. Unfortunately, it's found that direct dispensing of AuNR ink in the enhancement regions is not consistent for different concentration levels due to the physical properties of the AuNR ink (e.g. viscosity, surface tension) is not optimized for EPSON C88+ printer.

In this paper, we resorted to a low cost calligraphy method using a regular gel pen to dispense the AuNR ink on the QR assembly regions directly, as shown in Fig. 5(b). Similar procedure using a regular ballpoint pen to dispense AuNR solution was reported in our previous work [27], [28]. The original ink in the pen's refill container is pushed out using nitrogen gun after the tip and refill are separated. The gel pen refill and the tip are cleaned with ethanol by sonication for 2 days in a centrifuge tube. The ethanol is replaced every 3 hours until the color of ethanol doesn't change (no more ink gets dissolved in ethanol). Both the pen's refill container and the pen tip are dried with nitrogen gun. The AuNR solution is then injected into the cleaned gel pen refill and the pen is ready to dispense the AuNR ink solution in the QR assembling regions (Fig. 5(b) and (c)). Fig. 5(d) shows the side view and top view of the pen tip.

D. Measurement Results

1) Silver Enhancement on Different Paper Substrates: We have compared the process of self-assembly by calligraphing text (in this case "AIM LAB") with AuNR ink and developing it using silver enhancement technique on different substrates in the following experiment. Four different substrate materials – printing paper, Whatman filter paper, nitrocellulose membrane and bacterial cellulose – have been used and compared in this experiment. Same text has been patterned on these four substrates with AuNR at same concentration level and developed with silver enhancement solution as time progresses, as shown in Fig. 6. Before silver enhancement, text on four different samples are nearly invisible (Fig. 6 (a1), (b1), (c1), and (d1)) because AuNRs are in a dimension scale of nanometers and are too small to be visibly observed. After silver enhancement the printing paper substrate turns into dark quickly in 4 minutes, which makes the text unrecognizable, as shown in Fig. 6(a3). It is mainly because the chemical reagents contained in printer paper binder also facilitate silver reduction.

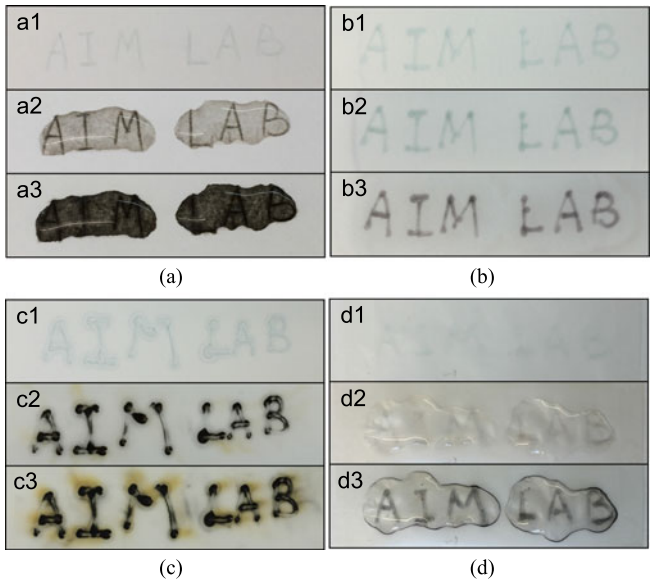

Fig. 6. Text calligraphed on four different substrates using AuNRs ink and developed with silver enhancement: (a1)–(a3) regular printing paper, before SE, 2 min and 4 min after SE, separately; (b1)–(b3) Whatman filter paper, before SE, 2 min and 7 min after SE; (c1)–(c3) nitrocellulose membrane, before SE, 2 min and 7 min after SE; (d1)–(d3) bacterial cellulose, before SE, 2 min and 7 min after SE.

Better results have been obtained on the other three substrates due to much less self-contained impurities. For instance, Whatman filter paper is only comprised of super-refined cellulose fibers. Calligraphed text on this substrate is legible after

7 minutes' silver enhancement (Fig. 6(b3)). However, during this process the applied silver enhancement solution spreads out and evaporates very quickly due to porous surface feature of filter paper. As a result, continuously adding silver enhancement solution on the filter paper is necessary to provide sufficient reagent to facilitate further silver deposition.

Similarly, nitrocellulose membrane is also highly porous (pore size in micrometers). As a result, continuously applying silver enhancement solution on the calligraphed text is necessary to promote further silver reduction. Although the text is legible after 7 minutes' silver enhancement on nitrocellulose membrane, part of the AuNRs are dispersed away from their original spots by the applied silver enhancement solution and they have also undergone silver enhancement process. As a result, the color of the adjacent area of the text becomes blotted and reduces the legibility of the text.

AuNR text on bacterial cellulose substrate is developed and remain clear and legible after 7 minutes' silver enhancement. Different from above mentioned substrates, bacterial cellulose could retain silver enhancement solution in the spot where it is originally applied since it is has a much smaller pore size (in nanometer scale). One time silver enhancement application is sufficient to develop the calligraphed text on the substrate. Note that there is a noticeable black line surrounding the silver enhancement solution drop after 7 minutes' development as shown in Fig. 6(d3) which is known as "coffee ring effect" [29]–[31]. Because of different evaporation rates across the silver enhancement solution drop, solution evaporated on the edge is replenished by the liquid from the interior. In this way, some AuNRs dispensed on the surface of the bacterial cellulose that are not firmly captured by the substrate surface are dispersed to the edge. In the meantime, these AuNRs are also exposed to the silver enhancement solution, and have undergone silver enhancement process.

The AuNRs retention capabilities of four different substrates have also been examined. The substrates are first immersed in the AuNRs solution with same concentration over night. Then they are gently rinsed with DI water and air dried. Surface morphologies before and after silver enhancement have been compared with SEM examination for different substrates, as shown in Fig. 7. AuNRs can be uniformly captured on the surface of Whatman filter paper, nitrocellulose and bacterial cellulose. With silver enhancement, metallic silver clusters have been formed on both printing paper and nitrocellulose substrates. Compared to other three cellulose substrates, the ultrafine nanoscale network feature of bacterial cellulose (shown in Fig. 7(d1) and (d2)) anchors the AuNR cored silver shelled particles in its 3D network, and hence provides higher retention capability.

2) QR Code Self-Assembly on Different Substrates: Self-assembling process of the proposed FEC biosensor prototype have also been validated on these four substrates as shown in Fig. 8. AuNRs solution with concentration of 4.13×10^{-9} M has been dispensed onto prototypes' self-assembling regions using a low cost calligraphy method as described in Section II-C. Self-assembling process occurs once the silver enhancement solution is applied to the regions where AuNRs have been patterned. However, in the case of printing paper not only AuNRs but also other chemical binders facilitate the silver ion reduction. As a result, silver deposition occurs in the region of substrate wherever exposed to the silver enhancement reagent, which makes the QR code undecodable in less than 4 minutes as shown in Fig. 8(a3).

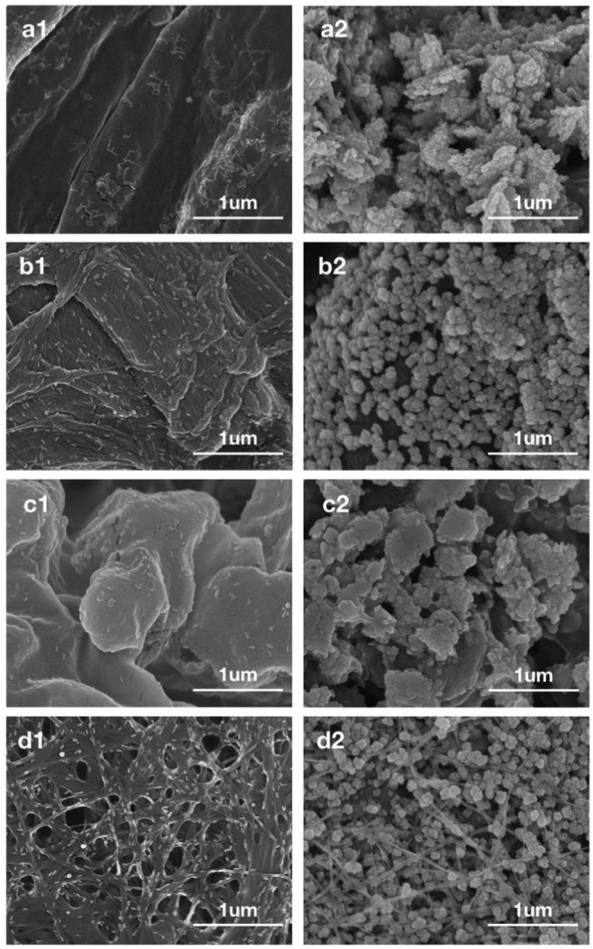

Fig. 7. SEM images showing AuNRs before and after 15 minutes' silver enhancement on different substrates (a1–a2: printing paper; b1–b2: Whatman filter paper; c1–c2: nitrocellulose; d1–d2: bacterial cellulose).

Although good text development result has been achieved on filter paper as shown in Fig. 6(b), filter substrate of the prototype gets yellow in the self-assembling process (Fig. 8(b2) and (b3)). The QR code deviates from a valid QR code, lies outside of the decoding radius and becomes a invalid code-word ultimately. This is because impurities contained in ink (used to print QR code) get dissolved in silver enhancement solution and have been dispersed off their original spots as silver enhancement solution spread out on the porous filter paper. As time progresses, more ink impurities get accumulated in the regions where black QR code modules are not printed. Silver ions get reduced and accumulates in those regions, which acts as the noise and corrupts the QR code ultimately. Same thing occurs on the nitrocellulose membrane based QR code biosensor prototype also because of its porous feature, as shown in Fig. 8(c1)–(c3).

Besides bacterial cellulose's high particle retention capability due to its ultrafine nanoscale network mentioned in

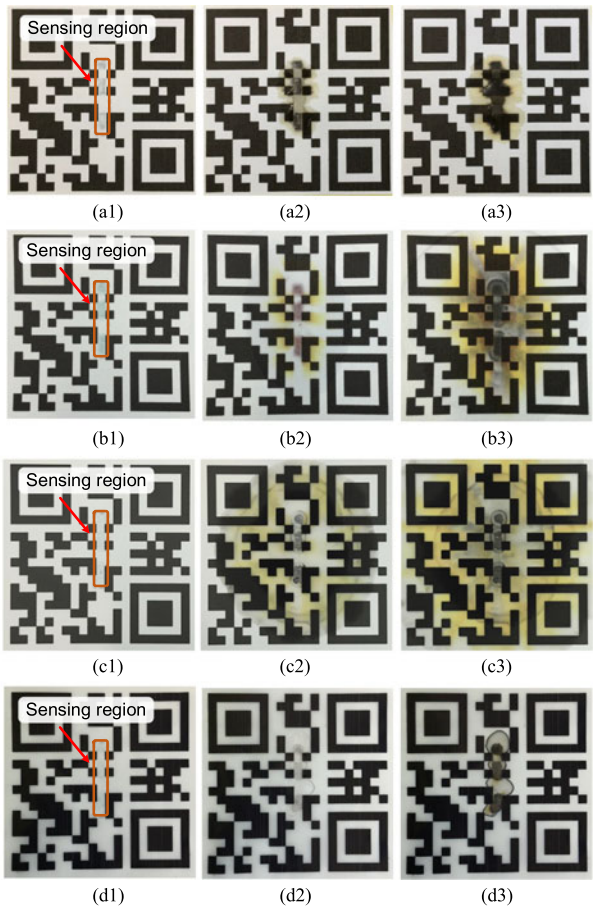

Fig. 8. QR code biosensor prototype using: (a1)–(a3) printing paper, before SE, 2 min and 4 min after SE, separately; (b1)–(b3) filter paper, before SE, 5 min and 15 min after SE; (c1)–(c3)nitrocellulose membrane, before SE, 5 min and 15 min after SE; (d1)–(d3) bacterial cellulose, before SE, 5 min and 15 min after SE.

Section II-D1, it also has advantages over previous substrates: 1) there's no impurities contained in the substrate can facilitate the silver enhancement; 2) it is not as porous as filter paper and nitrocellulose paper so that the applied silver enhancement solution can be retained in the spot where it is originally applied. Fig. 8(d3) shows the self-assembled FEC sensor using bacterial cellulose substrate after 15 minutes' self-assembling. The modules where AuNRs were dispensed have been successfully developed and in the meantime keep their neighborhood area intact. "Coffee ring effect" observed in Fig. 6(d3) persists in this case, as shown in Fig. 8(d3). Fortunately, due to the error correction capabilities embedded in the QR codes encoding process, it has little effect on the decoding process. QR code can be successfully decoded with a standard smart-phone and readers can verify this using their own smart-phones.

3) Quantitative Measurement Using QR Codes: We also verified whether the proposed sensing approach could be used to infer the concentration levels of target analytes. Three dilution levels (1:1, 1:3 and 1:9) of AuNR solution at the concentration of 4.13×10^{-9} M were prepared and dispensed in the self-assembling regions of QR code on bacterial cellulose. The time used to successfully decode the QR code after the silver-enhancement solution applied was measured for different dilution levels. Each measurement was repeated three times and the relative error-bars were also shown in Fig. 9. As it can be seen from Fig. 9, the QR code detection time, or assembly time increases monotonically with respect to the AuNR dilution levels, thus demonstrating the use of QR decoding for measuring concentration levels of target analytes.

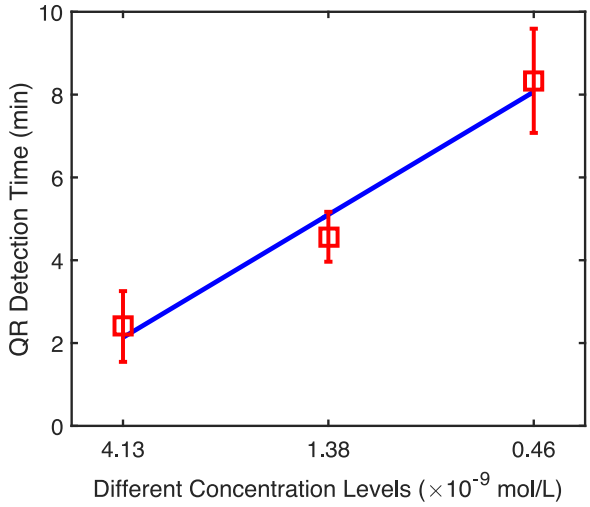

Fig. 9. Time measured to assemble the valid QR code using silver enhancement for different concentration levels of AuNR solution on the bacterial cellulose substrate.

III. Light Triggered Reagent Sampling

A. Operating Principle

In this section we describe an analyte sampling approach that is remotely triggered by light. Fig. 10(a) shows the operating principle using a prototype composed of a paper-based microfluidic network. A hydrophobic layer ensures that analyte flows in the predefined microfluidics channel region and prevents analyte leakage. A layer of graphite material is patterned at one end of the channel and the analyte is applied to the other end of the channel, as shown in Fig. 10(a). The graphite heating layer converts the incident light into heat and creates a thermal gradient across the channel. An increase in evaporation rate close to the graphite layer, as shown in Fig. 10(a), imposes a diffusive force on the analyte directed towards the sensing regions (e.g., labeled in Fig. 1) which can then be designed to be located along the microfluidic channel.

B. Prototype Fabrication

The proof-of-concept prototype fabrication process is depicted in Fig. 10(b)–(g). A lab Whatman filter paper with desired shape (2 cm × 3.5 cm rectangle shape in this case) is used as the prototype substrate, shown in Fig. 10(b). A layer of hydrophobic material (wax in this case) is patterned on the filter paper substrate to form the microfluidic channel region as shown in Fig. 10(c). The substrate is then heated at 125 °C for 1 minute to form a hydrophobic barrier inside its 3D-network of the cellulose, shown in Fig. 10(d). Channel region on the backside is then

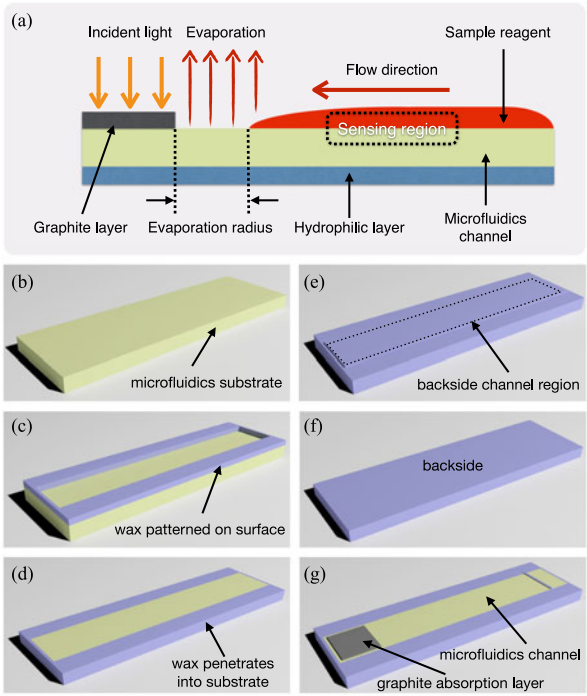

Fig. 10. (a) Principle of the proposed light triggered analyte sampling approach; (b)–(g) illustrate light triggered reagent sampling prototype fabrication process: (b) filter paper with desired shape and size; (c) patterned with hydrophobic layer on the surface; (d) channel formed by heating at 125 °C for 1 min; (e) patterned with hydrophobic layer on back side of channel area to prevent reagent from leaking; (f) heated at 80 °C for 5 sec; (g) graphite layer patterned.

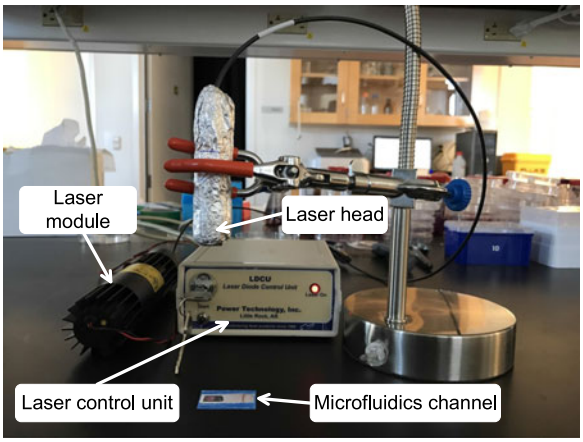

Fig. 11. Experimental setup showing the infrared laser light source.

also patterned with a layer of hydrophobic material (Fig. 10(e)) and heated at 80 °C for 5 seconds (Fig. 10(f)). In this manner, the liquid sample analyte can then freely flow in the microfluidic channel region on the front side without leaking from backside. Note that the time and temperature of this heating process at this step need to be carefully tuned such that front side will not be blocked by the wax. Lastly, a graphite layer is patterned on one end of the channel region by rubbing a standard pencil, shown in Fig. 10(g). When a light beam is focused on this graphite heating layer, the light can be efficiently converted into heat

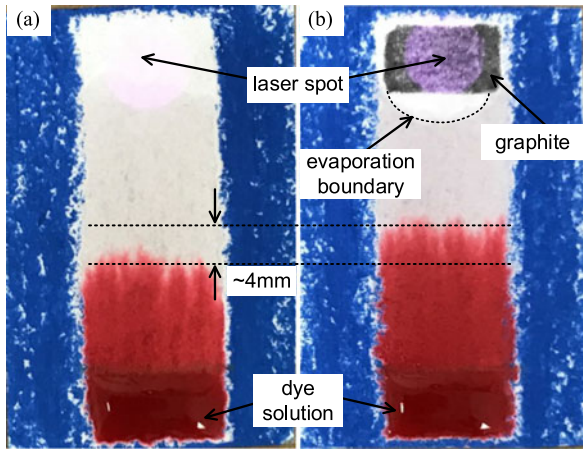

Fig. 12. Comparison of penetration lengths achieved by the dye solution in prototypes (a) without and (b) with graphite heating layer, 5 min after the solution was applied.

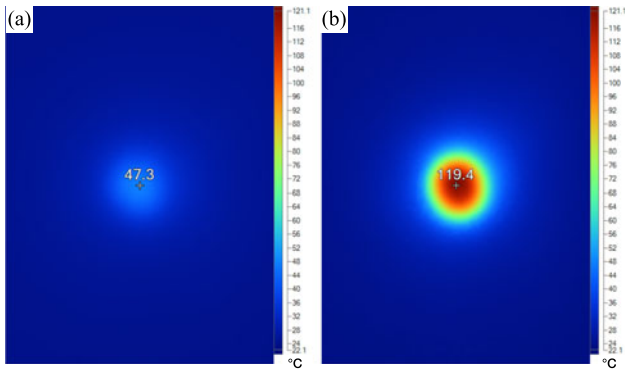

Fig. 13. Thermal images of the devices (a) without and (b) with graphite heating layer, when exposed to 300 mW 808 nm laser.

which can then create a thermal gradient to drive the flow of sample analyte.

C. Measurement Results

Two microfluidic channels were fabricated using the fabrication process shown in Fig. 12. One of the channels was chosen as a control and was not patterned with the graphite layer, as shown in Fig. 12(a). A red dye solution was chosen as a model analyte to visualize the flow through the microfluidic channel. The channel regions were initially filled with DI water. Thermal gradient was created by focusing a beam of 808 nm laser source in the region, labeled in Fig. 12(a) and (b). The experiment setup is shown in Fig. 11 where the distance between the laser head and graphite layer is carefully tuned such that 300 mW infrared is received at the laser spot. 50 μL red dye solution was then applied at the end of the microfluidics channel. Fig. 12 shows a comparison of dye solution propagation distances on two cases (with and without graphite layer) after 5 minutes of applying the dye solution. It can be clearly seen that the red dye solution propagates further on the channel with the graphite layer, thus verifying the light-based triggering hypothesis.

Fig. 13(a) and (b) show the thermal images of the laser spots labeled in Fig. 12 when exposed to a 300 mW 808 nm infrared

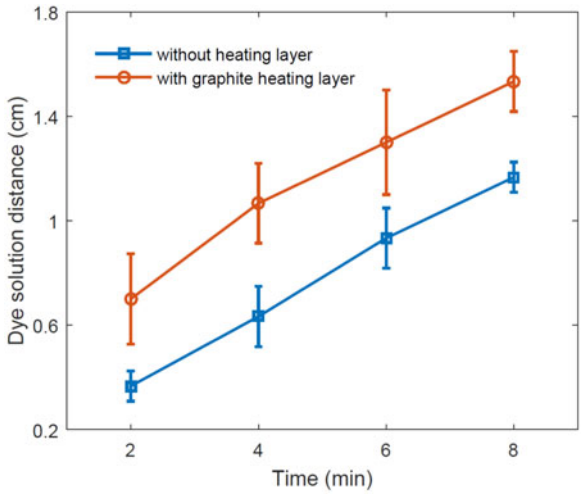

Fig. 14. Comparison of dye solution flow-rates without and with graphite heating layer.

laser. A 120 °C temperature is measured on the graphite coated substrate while only 50 °C is monitored for the case without graphite coating layer. This shows that light is more efficiently converted into heat with graphite heating layer and which then drives the flow of reagent. Fig. 14 compares the flow rate of dye solution on the microfluidics channels with and without graphite heating layer. A higher reagent flow rate is observed on the channel region patterned with graphite layer, which also verifies the proposed hypothesis.

IV. Conclusion

In this paper we addressed two challenges related to the integration of paper-based QR-code biosensors on liquid packages. We have compared four paper-based substrates for printing and assembling QR codes which includes regular printing paper, Whatman filter paper, nitrocellulose membrane and lab synthesized bacterial cellulose. Among these four different substrates, lab synthesized bacterial cellulose outperforms the other three. Although "coffee ring effect" occurs after the silver enhancement process, the assembled QR code can be correctly decoded due to the FEC capabilities embodied in the encoding process of the QR code. It also has been shown in the paper that QR code self-assembling time can be used to infer the target analyte concentration levels. In this paper we have also proposed a novel approach for automatic analyte sampling which can be triggered using a light source. A graphite heating layer is patterned on one end of the channel and is used for creating thermal gradient and hence concentration gradients when exposed to a light source. While the proof-of-concept operation was demonstrated using a 300 mW 808 nm laser source in this paper, a more practical choice would be to use light sources already available on smart-phones. However, the intensity of the smartphone LED light source might be too weak to trigger analyte sampling using the current prototype implementation. Fortunately, the following two methods could be used to boost the efficiency of sampling, which could be part of the future work: (a) engineer heating material (e.g., nanoparticles [32], [33], metamaterials [34], or polydopamine [35]) with high absorption characteristics to the smartphone LED light spectrum; or (b) use a lensing scheme to focus the LED light (e.g., Lens [36]) onto the graphite layer. While this paper has presented a preliminary prototype for proof-of-concept demonstration, future work would require integrating all the individual components, such as QR code platform (A in Fig. 1) and microfluidics channel (B in Fig. 1) together into a complete QR code biosensor where sample acquisition can be triggered with a light source.

Acknowledgment

The authors would like to thank Mr. Z. Wang for his contribution of TEM imaging of AuNR.

References

[1] A. K. Yetisen, M. S. Akram, and C. R. Lowe, "Paper-based microfluidic point-of-care diagnostic devices," *Lab Chip*, vol. 13, no. 12, pp. 2210–2251, 2013.
[2] J. Yu, L. Ge, J. Huang, S. Wang, and S. Ge, "Microfluidic paper-based chemiluminescence biosensor for simultaneous determination of glucose and uric acid," *Lab Chip*, vol. 11, no. 7, pp. 1286–1291, 2011.
[3] L. Ge, S. Wang, X. Song, S. Ge, and J. Yu, "3d origami-based multifunction-integrated immunodevice: Low-cost and multiplexed sandwich chemiluminescence immunoassay on microfluidic paper-based analytical device," *Lab Chip*, vol. 12, no. 17, pp. 3150–3158, 2012.
[4] A. W. Martinez, S. T. Phillips, G. M. Whitesides, and E. Carrilho, "Diagnostics for the developing world: Microfluidic paper-based analytical devices," *Anal. Chem.*, vol. 82, no. 1, pp. 3–10, 2009.
[5] A. W. Martinez, S. T. Phillips, and G. M. Whitesides, "Three-dimensional microfluidic devices fabricated in layered paper and tape," *Proc. Nat. Acad. Sci. USA*, vol. 105, no. 50, pp. 19 606–19 611, 2008.
[6] J. C. Jokerst, J. A. Adkins, B. Bisha, M. M. Mentele, L. D. Goodridge, and C. S. Henry, "Development of a paper-based analytical device for colorimetric detection of select foodborne pathogens," *Anal. Chem.*, vol. 84, no. 6, pp. 2900–2907, 2012.
[7] M. Yuan, E. C. Alocilja, and S. Chakrabartty, "A novel biosensor based on silver-enhanced self-assembled radio-frequency antennas," *IEEE Sensors J.*, vol. 14, no. 4, pp. 941–942, Apr. 2014.
[8] M. Yuan, E. C. Alocilja, and S. Chakrabartty, "Self-powered wireless biosensing based on integration of paper-based microfluidics with self-assembling RFID antennas," in *Proc. IEEE 2015 Proc. Biomed. Circuits Syst. Conf.*, 2015, pp. 1–4.
[9] M. Yuan, P. Chahal, E. C. Alocilja, and S. Chakrabartty, "Sensing by growing antennas: A novel approach for designing passive RFID based biosensors," in *Proc. 2015 IEEE Int. Symp. Circuits Syst.*, 2015, pp. 2121–2124.
[10] M. Yuan, K.-K. Liu, S. Singamaneni, and S. Chakrabartty, "Self-powered forward error-correcting biosensor based on integration of paper-based microfluidics and self-assembled quick response codes," *IEEE Trans. Biomed. Circuits Syst.*, vol. 10, no. 5, pp. 963–971, Oct. 2016.
[11] M. Yuan, P. Chahal, E. C. Alocilja, and S. Chakrabartty, "Wireless biosensing using silver-enhancement based self-assembled antennas in passive radio frequency identification (RFID) tags," *IEEE Sensors J.*, vol. 15, no. 8, pp. 4442–4450, Aug. 2015.
[12] M. Yuan, E. Alocilja, and S. Chakrabartty, "Self-powered wireless affinity-based biosensor based on integration of paper-based microfluidics and self-assembled RFID antennas," *IEEE Trans. Biomed. Circuits Syst.*, vol. 10, no. 4, pp. 799–806, Aug. 2016.
[13] W. Dungchai, O. Chailapakul, and C. S. Henry, "Electrochemical detection for paper-based microfluidics," *Anal. Chem.*, vol. 81, no. 14, pp. 5821–5826, 2009.
[14] S. Cinti, C. Minotti, D. Moscone, G. Palleschi, and F. Arduini, "Fully integrated ready-to-use paper-based electrochemical biosensor to detect nerve agents," *Biosensors Bioelectron.*, vol. 93, pp. 46–51, 2017.
[15] J. R. Choi, "An integrated paper-based sample-to-answer biosensor for nucleic acid testing at the point of care," *Lab Chip*, vol. 16, no. 3, pp. 611–621, 2016.
[16] M. M. Abeer, M. Amin, M. C. Iqbal, and C. Martin, "A review of bacterial cellulose-based drug delivery systems: Their biochemistry, current approaches and future prospects," *J. Pharmacy Pharmacol.*, vol. 66, no. 8, pp. 1047–1061, 2014.

[17] Z.-Y. Wu, H.-W. Liang, L.-F. Chen, B.-C. Hu, and S.-H. Yu, "Bacterial cellulose: A robust platform for design of three dimensional carbon-based functional nanomaterials," *Accounts Chem. Res.*, vol. 49, no. 1, pp. 96–105, 2015.
[18] D. Klemm *et al.*, "Nanocelluloses: A new family of nature-based materials," *Angewandte Chem. Int. Ed.*, vol. 50, no. 24, pp. 5438–5466, 2011.
[19] L. Tian, Q. Jiang, K.-K. Liu, J. Luan, R. R. Naik, and S. Singamaneni, "Bacterial nanocellulose-based flexible surface enhanced Raman scattering substrate," *Adv. Mater. Interfaces*, vol. 3, no. 15, Aug. 2016, Art. no. 1600214.
[20] Q. Jiang *et al.*, "Bilayered biofoam for highly efficient solar steam generation," *Adv. Mater.*, vol. 28, no. 42, pp. 9400–9407, 2016.
[21] J. Hu *et al.*, "Advances in paper-based point-of-care diagnostics," *Biosensors Bioelectron.*, vol. 54, pp. 585–597, 2014.
[22] M. Yuan, K.-K. Liu, S. Singamaneni, and S. Chakrabartty, "Analyte sampling in paper biosensors powered by graphite-based light absorption," in *Proc. 2017 IEEE Int. Symp. Circuits Syst.*, 2017, pp. 1–4.
[23] A. Gole and C. J. Murphy, "Azide-derivatized gold nanorods: Functional materials for click chemistry," *Langmuir*, vol. 24, no. 1, pp. 266–272, 2008.
[24] X. Huang, S. Neretina, and M. A. El-Sayed, "Gold nanorods: From synthesis and properties to biological and biomedical applications," *Adv. Mater.*, vol. 21, no. 48, pp. 4880–4910, 2009.
[25] J. V. Jokerst, A. J. Cole, D. Van de Sompel, and S. S. Gambhir, "Gold nanorods for ovarian cancer detection with photoacoustic imaging and resection guidance via raman imaging in living mice," *ACS Nano*, vol. 6, no. 11, pp. 10 366–10 377, 2012.
[26] L. Tian, E. Chen, N. Gandra, A. Abbas, and S. Singamaneni, "Gold nanorods as plasmonic nanotransducers: Distance-dependent refractive index sensitivity," *Langmuir*, vol. 28, no. 50, pp. 17 435–17 442, 2012.
[27] L. Tian *et al.*, "Bioplasmonic calligraphy for multiplexed label-free biodetection," *Biosensors Bioelectron.*, vol. 59, pp. 208–215, 2014.
[28] L. Tian *et al.*, "Multiplexed charge-selective surface enhanced raman scattering based on plasmonic calligraphy," *J. Mater. Chem. C*, vol. 2, no. 27, pp. 5438–5446, 2014.
[29] R. D. Deegan, O. Bakajin, T. F. Dupont, G. Huber, S. R. Nagel, and T. A. Witten, "Capillary flow as the cause of ring stains from dried liquid drops," *Nature*, vol. 389, no. 6653, pp. 827–829, 1997.
[30] H. Hu and R. G. Larson, "Evaporation of a sessile droplet on a substrate," *J. Phys. Chem. B*, vol. 106, no. 6, pp. 1334–1344, 2002.
[31] P. J. Yunker, T. Still, M. A. Lohr, and A. Yodh, "Suppression of the coffee-ring effect by shape-dependent capillary interactions," *Nature*, vol. 476, no. 7360, pp. 308–311, 2011.
[32] A. O. Govorov and H. H. Richardson, "Generating heat with metal nanoparticles," *Nano Today*, vol. 2, no. 1, pp. 30–38, 2007.
[33] E. A. Coronado, E. R. Encina, and F. D. Stefani, "Optical properties of metallic nanoparticles: Manipulating light, heat and forces at the nanoscale," *Nanoscale*, vol. 3, no. 10, pp. 4042–4059, 2011.
[34] J. Hao, L. Zhou, and M. Qiu, "Nearly total absorption of light and heat generation by plasmonic metamaterials," *Phys. Rev. B*, vol. 83, no. 16, 2011, Art. no. 165107.
[35] Q. Jiang, H. G. Derami, D. Ghim, S. Cao, Y.-S. Jun, and S. Singamaneni, "Polydopamine-filled bacterial nanocellulose as a biodegradable interfacial photothermal evaporator for highly efficient solar steam generation," *J. Mater. Chem. A*, vol. 5, no. 35, pp. 18397–18402, 2017.
[36] F. Lens, The first flashlight booster for smartphones, 2016. [Online]. Available: http://www.relio.it/flens

Mingquan Yuan (S'14) received the B.S. degree in electronic science and technology from Huazhong University of Science and Technology, Wuhan, China, in 2009, and the M.S. degree in electronics engineering and computer science from Peking University, Beijing, China, in 2012. He is currently working toward the Ph.D. degree at Washington University in St. Louis, St. Louis, MO, USA.

From 2012 to 2015, he was a Research Assistant with Michigan State University, East Lansing, MI, USA. His research interests include passive RFID biosensors, wireless detection, flexible electronics, microfluidics, and microfabrication/nanofabrication.

Qisheng Jiang received the B.S. degree in materials processing engineering from the Beijing Institute of Technology, Beijing, China, in 2013, and the M.S. degree in materials science and engineering from Washington University in St. Louis, St. Louis, MO, USA, in 2014. He is currently working toward the Ph.D. degree at Washington University in St. Louis. His research interests include paper-based sensors and functional materials based on bacterial nanocellulose for various applications including water purification and energy storage.

Keng-Ku Liu received the B.S. and M.S. degrees from the National Tsing Hua University, Hsinchu, Taiwan, in 2006 and 2009, respectively, and the Ph.D. degree in materials science and engineering from Washington University in St. Louis, St. Louis, MO, USA, in 2017. His research interests include the synthesis and characterizations of low-dimensional nanomaterials and their applications.

Srikanth Singamaneni received the B.Tech. degree from Nagarjuna University, New Delhi, India, in 2002, the M.S. degree in electrical and computer engineering from Western Michigan University, Kalamazoo, MI, USA, in 2004, and the Ph.D. degree in polymer materials science and engineering from Georgia Institute of Technology, Atlanta, GA, USA, in 2009. He is currently an Associate Professor with the Department of Mechanical Engineering and Materials Science, Washington University in St. Louis, St. Louis, MO, USA. His work involves the design and synthesis of a wide variety of metal nanostructures and organic/inorganic hybrids and their application in chemical and biological sensors and nanotheranostics. He is the recipient of the National Science Foundations CAREER award, the Deans Faculty Award for Innovation in Research, and the Graduate Student GOLD award from Materials Research Society.

Shantanu Chakrabartty (S'99–M'04–SM'09) received the B.Tech degree from the Indian Institute of Technology, Delhi, New Delhi, India in 1996, and the M.S and Ph.D degrees in electrical engineering from Johns Hopkins University, Baltimore, MD in 2002 and 2004 respectively. He is currently a Professor with the Department of Computer Science and Engineering, Washington University in St. Louis, St. Louis, MO, USA. From 2004 to 2015, he was an Associate Professor with the Department of Electrical and Computer Engineering, Michigan State University (MSU), East Lansing, MI, USA. From 1996 to 1999, he was with Qualcomm Incorporated, San Diego CA, USA, and he was a visiting Researcher with The University of Tokyo in 2002. His work covers different aspects of analog computing, in particular nonvolatile circuits. His research interests include energy harvesting sensors and neuromorphic and hybrid circuits and systems. He is currently an Associate Editor for the IEEE TRANSACTIONS OF BIOMEDICAL CIRCUITS AND SYSTEMS, an Associate Editor for the *Advances in Artificial Neural Systems* journal, and a Review Editor for *Frontiers of Neuromorphic Engineering* journal. He was a Catalyst foundation fellow from 1999 to 2004 and was the recipient of the National Science Foundation's CAREER award, the University Teacher-Scholar Award from MSU, and the 2012 Technology of the Year Award from MSU Technologies.